RELATIVE CONTRIBUTION OF DIFFERENT BONDING MECHANISMS DURING THE FFF PROCESS

Shokrollahi, M[1]*, Dubé, M[1], and Tabiai, I[1]
[1] CREPEC, Département de génie mécanique, École de Technologie Supérieure, Montréal, Canada
* Corresponding author (maryam.shokrollahi.1@ens.etsmtl.ca)

Keywords*: FFF, Bonding mechanism, Bonding strength*

1 ABSTRACT

Fused Filament Fabrication (FFF), also known as Fused Deposition Modeling (FDM), is the most widely used additive manufacturing technique. This process involves a movable heated nozzle, through which a molten thermoplastic polymer fibre is extruded onto a platform. Deposited filaments bond together and solidify to form a layer, and successive layers are extruded on top of each other to complete the final part. Layer by layer deposition of the material and incomplete bonding between the filaments leads to inferior mechanical properties of FFF printed parts, relative to the mechanical properties of the bulk material. This limits the adoption of FFF technology in the industry. To address this problem, a better understanding of the bonding process is necessary. Recently, it was proposed that the pressure applied on the previous layer by the extruded filament controls the bonding strength [1]. However, the sintering (i.e. pressureless bonding mechanism) could also be driving the interfacial strength [2]. The work presented here is an attempt to determine the relative contribution of each bonding mechanism in the FFF process. Two sets of samples (one filament thick) with the same processing parameters and geometry are printed with two different strategies. The bonding process is controlled by sintering in one set, while both sintering and pressure-driven bonding contribute in the other set of samples. Microtensile tests are conducted to evaluate the bonding strength of the samples. The comparison of the bonding strength was not possible due to an invalid failure mode in the second set of samples. However, the stiffness values obtained using data from the elastic region of stress versus strain curves, show no difference between the two sets.

2 INTRODUCTION

Fused Filament Fabrication (FFF), also called Fused Deposition Modeling (FDM), is a technology of layer-by-layer deposition of thermoplastic polymers to manufacture objects from computer-aided design (CAD) data. As the most popular and the most widely used AM technology, it has recently gained more interest in several industries. However, one of the main challenges limiting its adoption is the poor interlayer bonding between the printed filaments. The structural integrity of FDM parts is determined by the quality of the bond interface between the filaments and layers. Surface adhesion and molecular diffusion between neighbouring deposited filaments are required for bonding in polymer systems [3].

The bonding mechanism between the filaments has been modelled in different ways. Diffusion models are widely used to describe this phenomenon, showing that the interlayer strength increases as the polymer macromolecules diffuse across the interface [3, 4]. However, interlayer contact should also be considered to develop an effective and accurate model, since it affects the subsequent steps of the bonding process [4]. Currently, there are two approaches to describe how the interlayer contact happens between adjacent filaments. Some researchers employ sintering models to describe the bonding process. In this point of view, surface tension between the two filaments

initiates interlayer contact [2, 5]. However, it was recently proposed that the pressure applied on the previous layer by the extruded filament controls the bonding strength [1,4]. In other words, the intimate contact between the filaments, which is defined as surface rearrangement and surface approach, is pressure-driven. Figure 1, schematically shows the bonding between two filaments printed side by side or on top of each other when assuming that the bonding process is controlled either by sintering or by contact pressure.

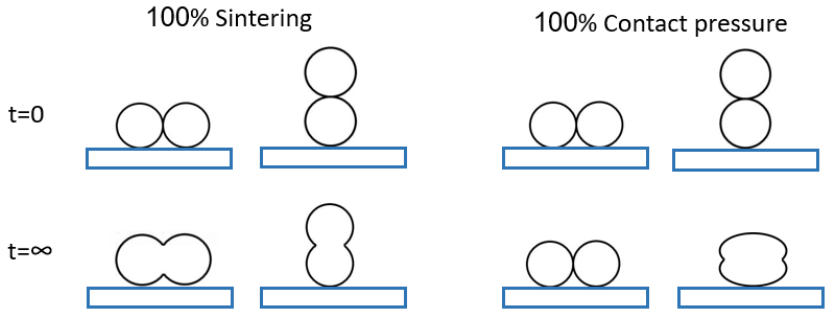

Figure 1. Filament bonding schematic dominated by two bonding mechanisms. Each circle represents the cross-section of a printed filament. Two print strategies are considered for each case. If contact is achieved by sintering (100% sintering), the same bonding quality is obtained, whether the filaments are printed on top of each other or next to each other. However, if contact is achieved by pressure (100% contact pressure), bonding happens only when the filaments are printed on top of each other. In effect, there is almost no contact pressure when filaments are deposited next to each other, while the contact pressure would be maximum when the filaments are printed on top of each other.

The bonding mechanism between the filaments during printing is probably driven by both sintering and contact pressure. However, to the best of our knowledge, there is no method to determine the dominant bonding mechanism during printing. The relative contribution of each mechanism is important because polymers do not behave the same in sintering or pressure-driven bonding condition. Therefore, determining the dominant bonding mechanism during printing for each polymer can be used to optimize the printing process for a certain polymer. This might ease the printing process of polymers that are difficult to print as well as improve the print quality of the parts with commonly used polymers.

3 EXPERIMENTAL METHODS

3.1 Printing

Small sheets in the form of 10 mm × 12 mm rectangles were printed with two different strategies. As depicted in Figure 2, the first set of samples was printed on the bed, in the X-direction. The filaments were printed next to each other in this case. Therefore, there is almost no contact pressure between the filaments and they will bond together through sintering. This set is called X-sheets. The second set of sheets are printed with the same printing parameters, but in the Z direction and they are called Z-sheets. In this case, filaments are printed on top of each other, leading to maximum contact pressure. The third set of samples was also printed in the Z direction. However, the surfaces of the sheets were sanded to reduce the cross-section area by more than three times. This set is called SZ-sheets, and is schematically shown in Figure 3. The arrows in Figure 2 represent the heat transfer mechanisms during the print. The heat transfer is not the same in X-sheets and Z-sheets. A heated bed is usually used during the print, and the heat conduction with the heated bed affects the quality of the part. However, in this experiment, a heated bed would have caused a significant difference in the thermal history of the samples. All filaments printed in X-sheets are in contact with the bed, while only one filament is printed on the bed in the Z-sheets. Therefore, the bed was kept at room temperature to reduce the differences in the thermal history of the samples. However, there were still

differences in thermal conditions, since Z-sheets were cooled mainly by convection, while conduction cooling had a more significant effect during the cooling of X-sheets.

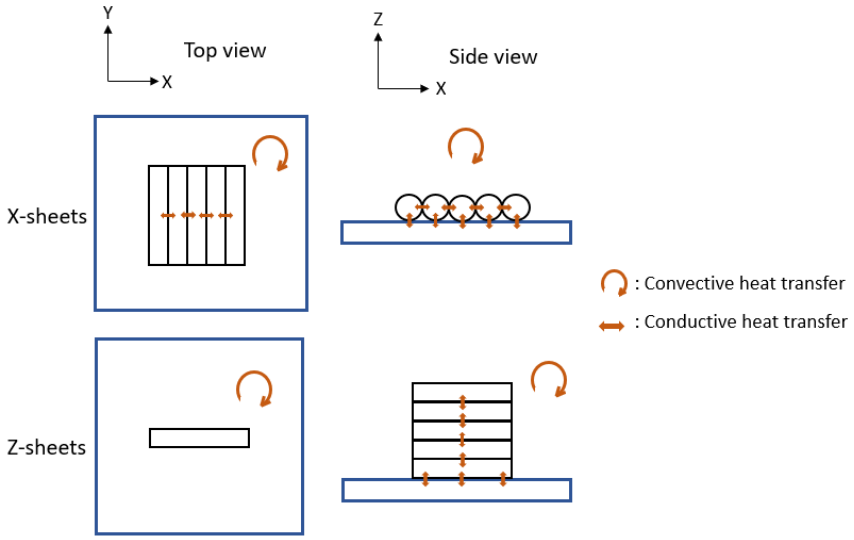

Figure 2. The schematic of the top and side view for the two different sets of samples. The print bed is depicted in blue. Conduction heat transfer occurs between the filaments as well as between the filaments and the bed, which is at room temperature. Convective heat transfer with the room environment also cools down the filaments.

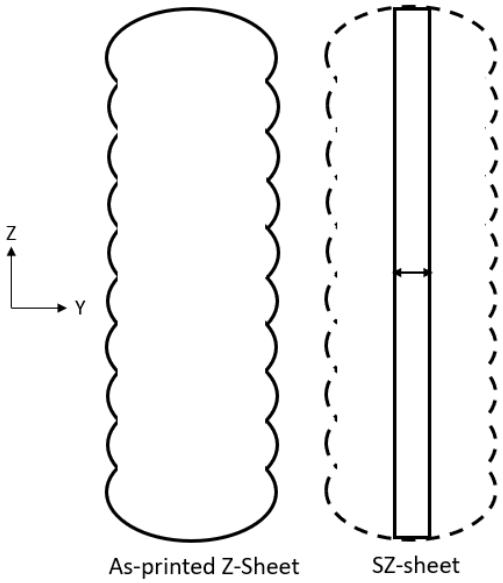

Figure 3. The schematic of Z-sheet (left) and SZ-sheets (right). The width of the filaments was decreased by more than three times after sanding.

Polylactic acid (PLA) filament with diameter of 1.75 mm, manufactured by Econofil was used as the printing material. The samples were printed using an Ender-3 printer manufactured by Creality3D, with a nozzle diameter of 0.4 mm.

Printing parameters were selected according to Table 1. It should be noted that retraction calibration was done before the print, and the optimal printing temperature for the polymer is determined during the calibration steps.

Table 1. Printing parameters for all sets of samples

Parameter	Printing temperature °C	Bed temperature °C	Filament thickness mm	Filament width mm	Printing speed mm/s
	200	25	0.2	0.4	15

3.2 Micro-tensile test

A micro-tensile testing device manufactured by *Kammrath and Weiss Systems* was used to conduct tensile experiments. Figure 4 illustrates the experimental setup used here. The displacement speed was set to 1500 µm/min for all tests. The applied force and the initial measured bonded area of the sheet were used to calculate stress. This area would be the filament thickness by the filament length, and the filament width by the filament length for X-sheets and Z-sheets respectively. It should be noted that the slight curvature of the filaments on the surface of the sheets as well as the caliper measurement errors prevent from obtaining the accurate effective bonded area. However, the error is too small to noticeably affect the results. The strain was obtained by the initial measured length of the sheets and the displacement of the crosshead.

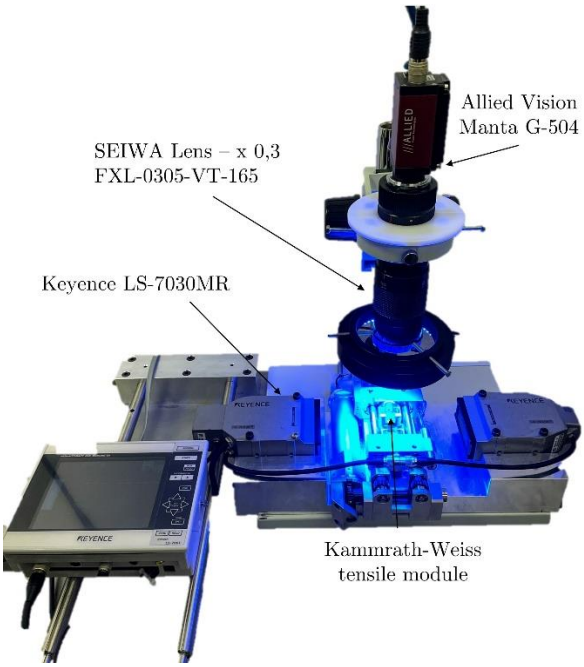

Figure 4. The microtensile device used to conduct tensile tests [6]. Each specimen was loaded in the tensile module with a displacement speed of 1500 µm/min. The camera on top of the sample captured one picture per second.

To mount the tensile specimens, each sheet was glued to two printed tabs, that were specifically made to fit the tensile machine requirements as well as the clamping system. These tensile specimens are schematically shown in Figure 5. In all cases, the load direction was perpendicular to the filaments. Therefore, the bonding strength could be evaluated during the tensile test.

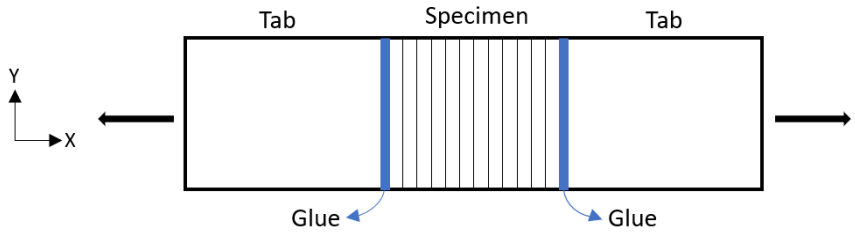

Figure 5. Schematic of tensile specimens. Black arrows show the loading direction, which is perpendicular to the filament direction.

4 RESULTS & DISCUSSION

4.1 Dimensional Evaluation

A caliper was used to measure the dimensions of the sheets after the print. The measured values were then used to calculate the filament width and thickness, using the total number of filaments in each sheet. The obtained values are presented in Table 2. The values set as the printing parameters in the *Cura* slicer software are referred to as prescribed values, and they are compared with the measurement after the print. The distance between the adjacent filaments in X-sheets are controlled by the infill line distance parameter; when it is equal to the prescribed filament width, there would be neither gap nor overlap between the adjacent filaments and they would be placed exactly next to each other. The width of the filaments in the X-sheets is very close to the prescribed value, while the filament thickness is larger than that. The opposite is observed for Z-sheets; the thickness of the filaments is almost equal to the prescribed value, while the width is increased more than two times. This significant increase in the filament width is due to the pressure applied during the print. The results imply that the shape deformation of printed filaments is highly affected by the position of their adjacent filaments.

Table 2. Prescribed and measured values of filament width and thickness for X-sheets and Z-sheets. Infill line distance determines the distance between the adjacent filaments. This parameter is not defined for Z-sheets since the filaments are printed on top of each other.

Sample	Prescribed Filament thickness mm	Prescribed filament width mm	Infill line distance mm	Measured filament thickness mm	Measured Filament width mm
X-sheets	0.2	0.4	0.4	0.32±0.03	0.38±0.02
Z-sheets	0.2	0.4	-	0.19±0.01	0.85±0.01

4.2 Microtensile Test Results

All tested X-sheets led to a valid failure mode, i.e., specimens debonded somewhere on the sheets, away from the tabs, and not between the sheets and the tabs. Figure 6 shows the stress-strain curve of the X-sheets. According to the curves, the debonding strength of the X-sheets is 18.2 ±1.7 MPa.

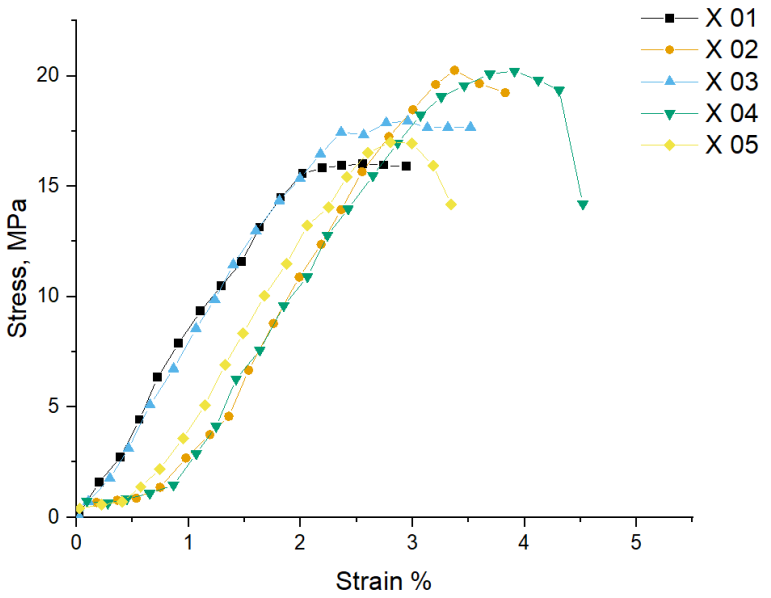

Figure 6. Stress as a function of strain curves for X-sheets. The maximum achieved stress is considered as the bond strength since the sample started debonding at this point.

Figure 7 shows the damage mechanism during the test. It can be seen that a crack first appeared in the middle of the sheet (Figure 7.b). When the crack length reached a certain value, a second crack was initiated near the first one (Figure 7.c). The cracks then grew until complete failure (Figure 7.d).

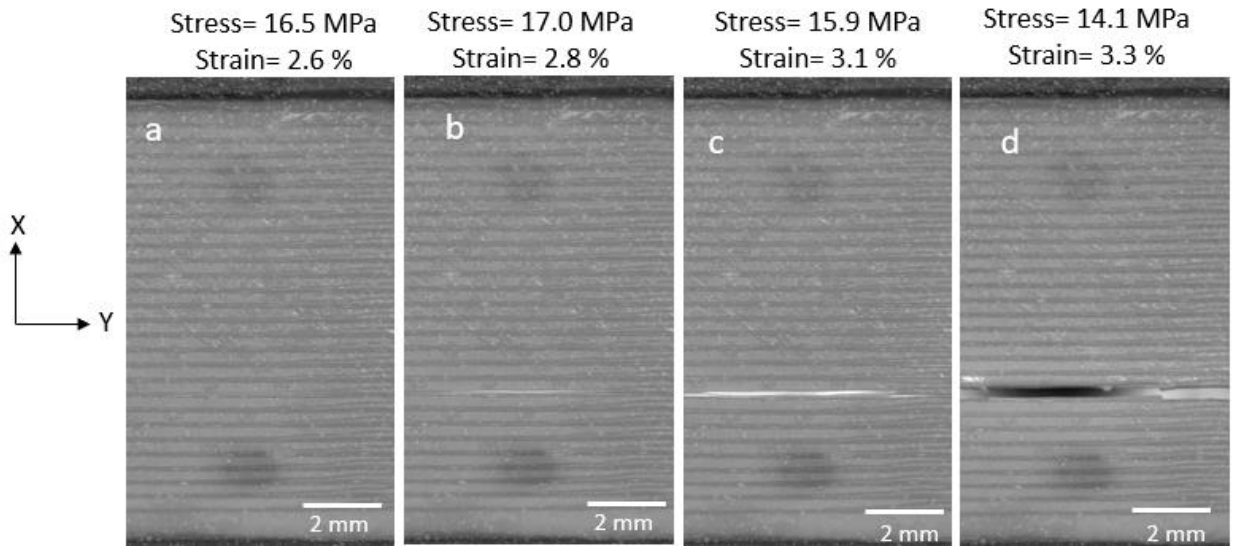

Figure 7. Damage mechanism evolution for X-02 sample during the tensile test. The specimen was loaded along the X direction. (b) A small crack appeared in the middle, and grew gradually. The second crack (c) appeared once the first crack reached a certain length. (d) The cracks then joined, and fracture occurred.

Z-sheets tensile tests, however, were not successful in that failure occurred between the sheet and the tabs. To address this problem, another set of Z-sheets was printed and sanded to decrease the specimens' cross-section. Therefore, less force would be needed to break the filaments. However, it did not solve the problem, and the breakage occurred again at the tabs' attachment.

Although the tensile tests for Z-sheets were not successful, it is still possible to compare the three sets of samples in the elastic region. The stiffness is calculated according to the ASTM D638 standard, and the obtained values are shown in Figure 8. There is no significant difference in stiffness between the X-sheets and Z-sheets. However, the stiffness increased by about 50 % for the SZ-sheets.

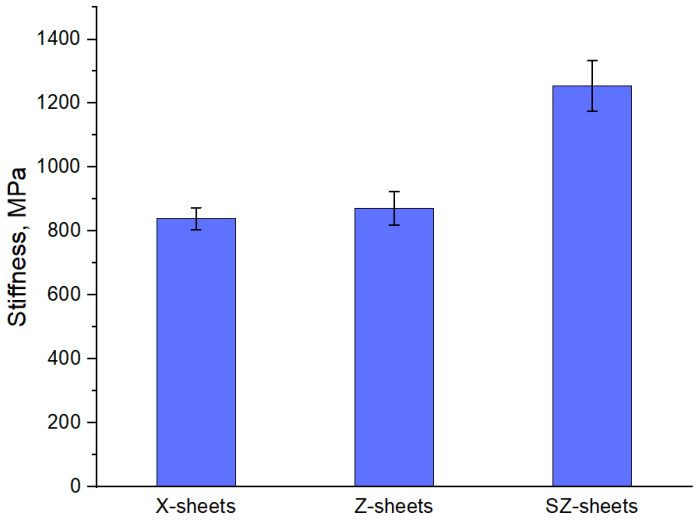

Figure 8. Stiffness values for each set of samples. ZS-sheets show higher stiffness, while no difference is observed between X-sheets and Z-sheets.

The stiffness of the samples is a superposition of the filament's stiffness and the bond's stiffness. The filament and bond properties are not expected to be homogenous through the filament's cross-section. Negligible difference in the stiffness of X-sheets and Z-sheets suggests that despite the possible different bonding mechanisms, the stiffness of the bond is the same in both sets. Another possibility is that the stiffness of the sheets is driven mostly by the filament properties rather than the bonding. Higher stiffness in SZ-sheets can be explained by non-uniform cooling rate along the cross-section. As schematically shown in Figure 9, the cooling rate at the edges of the contact area between two filaments is higher than the cooling rate in the middle of the area. Therefore, the middle of the cross-section stays at higher temperatures for a longer time. This would promote more molecular diffusion in this region, and possible higher stiffness. In addition, it is reported that the filament microstructure also varies along the cross section of printed filaments for semi crystalline polymers [8]. However, more experiments are required to investigate this effect here.

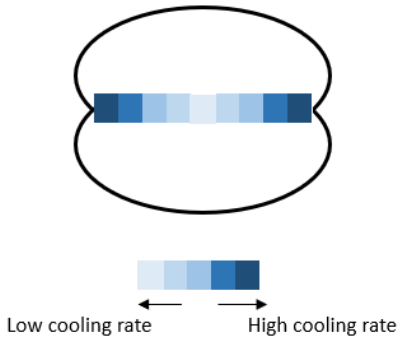

Figure 9. Schematic of the cooling rate variation along the cross-section of the bond between two filaments in Z-sheets. The middle area cools down more slowly compared to the edges, leading to more diffusion and higher stiffness.

4.3 Improvements

The methodology can be modified in different ways to obtain the correct bond strength value for Z-sheets. The bonding between the tabs and the sample can be improved by different methods. The sample geometry can also be modified by making the sheets thinner in the middle through curved edges. Moreover, it might be possible to print integrated samples using pre-printed supports. Therefore, no additional step would be required to prepare tensile specimens.

In terms of thermal conditions, X-sheets can be printed by bridging over empty space (i.e. printing over short distances without underlaying support material) instead of printing on a non-heated surface. This would further decrease the heat transfer differences between the two sets of sheets. As shown in Figure 2, conductive heat transfer occurs for X-sheets, while Z=sheets touch the bed only at the first layer. The conductive heat transfer with the print bed would be eliminated by bridging, and the filaments would cool down through convective heat transfer as it is the dominant heat transfer mechanism in Z-sheets as well.

Digital Image Correlation (DIC) would also be employed to more accurately analyze the micro-tensile test data. Several frames of the sheets under mechanical loading would be captured and analyzed using a DIC algorithm. In this method, the displacement would be obtained directly on the specimens, resulting in more accurate strain values. Moreover, DIC would provide a better understanding of the local bonding properties and the damage mechanisms by illustrating the strain concentration regions.

5 CONCLUSION

A new methodology is proposed to determine the relative contribution of the two main mechanisms responsible for filaments bonding during FFF. Two sets of samples with the same processing parameters and geometry were printed with two different strategies. The bonding process was controlled by sintering in one set, while both sintering and pressure-driven bonding contributed in the other set of samples. Microtensile tests were conducted to evaluate the bonding strength of the samples. The bonding strength in the first set was found to be 18.2 MPa. However, the bonding strength for the other set was not obtained due to the invalid fracture mode of the samples. As an attempt to address this problem, a new set of samples was introduced in which surfaces on both sides were sanded to decrease the cross-section area. Despite the fracture mode being still invalid in the new set, the stiffness increased by about 50%, while the first two sets behaved the same in the elastic region of the stress-strain curves. It seems that non-uniform bonding properties along the cross-section in the main reason for the observed difference

in the stiffness values. Lower cooling rate in the middle of the filaments probably results in a stronger bond formation and higher stiffness.

6 REFERENCES

[1] S. K. Kim, & al., "Non-Newtonian modeling of contact pressure in fused filament fabrication," *Journal of Rheology*, Vol. 65, No. 1, pp. 27–42, Dec, 2020.

[2] R. Lou, H. Li, J. Zhong, C. Zhang and D. Fang. "A transient updated Lagrangian finite element formulation for bond formation in fused deposition modeling process". *Journal of the Mechanics and Physics of Solids,* Vol. 152, 104450, 2021.

[3] Q. Sun, G. M. Rizvi, C. T. Bellehumeur and P. Gu. "Effect of processing conditions on the bonding quality of FDM polymer filaments". *Rapid prototyping journal,* Vol. 14, No. 2, pp 72–80, 2008.

[4] J. T. Coogan and D. O Kazmer. "Bond and part strength in fused deposition modeling". *Rapid Prototyping Journal*, Vol. 23, Issue 2, pp.414-422, 2017.

[5] L. Li, Q. Sun, C. Bellehumeur, and P. Gu. "Investigation of bond formation in FDM process". *International Solid Freeform Fabrication Symposium*, 2002.

[6] L. Catar, I. Tabiai, D. St-Onge, "Micro-tensile test machine and setup. figshare. Figure. https://doi.org/10.6084/m9.figshare.19492121.v1", 2022.

[7] N. R. Fry, R. C. Richardson, J. H. Boyle, "Robotic additive manufacturing system for dynamic build orientations". *Rapid Prototyping Journal*, Vol. 26, No. 4. pp. 659-667, 2020

[8] A. Nogales, E. Gutiérrez-Fernández, M.C. García-Gutiérrez, et al. "Structure development in polymers during fused filament fabrication (FFF): an in situ small-and wide-angle X-ray scattering study using synchrotron radiation". *Macromolecules*, Vol. 52, No. 24, pp.9715-9723, 2019.